Single-Shot Readout of a Nuclear Spin Weakly Coupled to a Nitrogen-Vacancy Center at Room Temperature

Gang-Qin Liu,[1,2] Jian Xing,[1] Wen-Long Ma,[2] Ping Wang,[3,2] Chang-Hao Li,[1] Hoi Chun Po,[2] Yu-Ran Zhang,[1] Heng Fan,[1,4] Ren-Bao Liu,[2,5,6] and Xin-Yu Pan[1,4,*]

[1]*Beijing National Laboratory for Condensed Matter Physics, Institute of Physics, Chinese Academy of Sciences, Beijing 100190, China*

[2]*Department of Physics, The Chinese University of Hong Kong, Shatin, New Territories, Hong Kong, China*

[3]*Beijing Computational Science Research Center, Beijing 100084, China*

[4]*Collaborative Innovation Center of Quantum Matter, Beijing 100871, China*

[5]*Centre for Quantum Coherence, The Chinese University of Hong Kong, Shatin, New Territories, Hong Kong, China*

[6]*The Chinese University of Hong Kong Shenzhen Research Institute, Shenzhen 518100, China*

(Received 23 February 2016; revised manuscript received 13 February 2017; published 12 April 2017)

Single-shot readout of qubits is required for scalable quantum computing. Nuclear spins are superb quantum memories due to their long coherence time, but are difficult to be read out in a single shot due to their weak interaction with probes. Here we demonstrate single-shot readout of a weakly coupled ^{13}C nuclear spin at room temperature, which is unresolvable in traditional protocols. States of the weakly coupled nuclear spin are trapped and read out projectively by sequential weak measurements, which are implemented by dynamical decoupling pulses. A nuclear spin coupled to the nitrogen-vacancy (NV) center with strength 330 kHz is read out in 200 ms with a fidelity of 95.5%. This work provides a general protocol for single-shot readout of weakly coupled qubits at room temperature and therefore largely extends the range of physical systems for scalable quantum computing.

DOI: 10.1103/PhysRevLett.118.150504

Nuclear spins in solids have been proposed as a promising candidate for quantum computing [1–3]. Quantum memory with ultralong coherence time [4–6], multiparticle entanglement [7–9], and real-time feedback control [10] have been demonstrated in nuclear spin systems. However, due to their small magnetic moments, it remains challenging to address and read out individual nuclear spins with high fidelity. To meet this challenge, usually a nearby electron spin is employed as an ancillary qubit. The readout fidelity of the target nuclear spin is then limited by the ancillary qubit. Taking nuclear spin around a nitrogen-vacancy (NV) center in diamond as an example, due to the low photon collection efficiency of the NV center, more than 10^5 repetitions of the readout sequence are needed to get a sufficient signal to noise ratio [3,11].

Even more challenging is single-shot readout of individual nuclear spins, which is a prerequisite of scalable quantum computing [12,13]. At cryogenic temperature, this can be achieved by mapping the nuclear spin state onto and subsequently projective readout of the electron spin with resonant optical excitation techniques [14–19]. At room temperature, however, spin mixing in the excited states prevents the resonant readout scheme, and single-shot readout is achieved only for strongly coupled nuclear spins [2,4,20,21]. For remote nuclear spins, their coupling strength is too weak to be resolvable in the noisy environment, and the controlled gate for the single-shot readout scheme cannot be implemented by traditional protocols, as shown in Fig. 1(a). As a result, the merits of weakly coupled nuclear spins, including their strength in numbers and less affected coherence by the ancillary electron spin, are less exploited.

In this Letter, we propose and demonstrate a scheme to achieve single-shot readout of weakly coupled nuclear spins at room temperature. This work is inspired by the scheme of dynamical decoupling (DD) enabled quantum sensing of weakly coupled nuclear spins via optically detected magnetic resonance (ODMR) of NV centers in diamond [22–26]. We will show that the DD sequence acts as a controllable quantum measurement on those weakly coupled nuclear spins, and illustrate that a set of nuclear spin basis states are stable under a repetitively applied DD sequence and nonresonant optical readout, which enables the single-shot readout scheme at room temperature.

The Hamiltonian of the NV electron spin and a weakly coupled ^{13}C nuclear spin $\hat{\mathbf{I}}$ under an external magnetic field $\mathbf{B}$ is [27,28]

$$H = S_z \otimes (\mathbf{A}\cdot\hat{\mathbf{I}}) - \gamma_n \mathbf{B}\cdot\hat{\mathbf{I}}, \tag{1}$$

where the NV spin-1 S_z has eigenstates $\{|0\rangle, |\pm 1\rangle\}$, $\mathbf{A}$ is the hyperfine interaction, and γ_n is the gyromagnetic ratio of ^{13}C nuclear spins. Note that we have dropped the zero field splitting and Zeeman terms of the electron spin since they have no effects in this pure-dephasing model. This Hamiltonian can be recast into the subspace $\{|0\rangle, |-1\rangle\}$ as

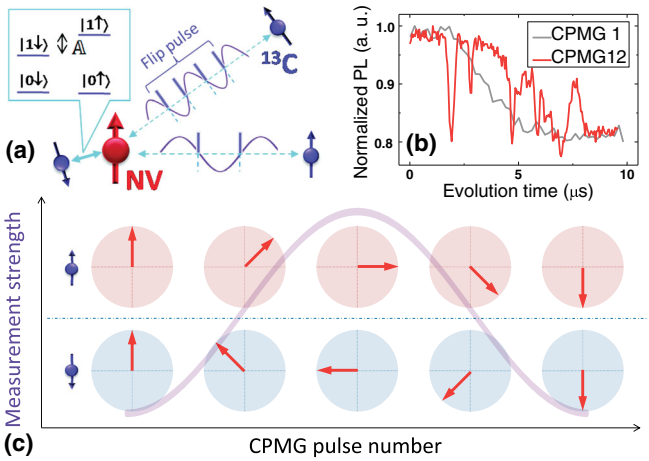

FIG. 1. System and experimental scheme for dynamical decoupling enabled quantum measurement. (a) An NV electron spin (red) and its ^{13}C nuclear spin bath (purple). The spin state of a strongly coupled ^{13}C nuclear spin can be mapped to the electron spin through selective MW pulses. For weakly coupled nuclear spins, DD is employed to address the target one while decoupling the other nuclear spins. (b) Coherence of the center electron spin under CPMG-12 (red line) and CPMG-1 (gray line), as a function of the pulse interval τ. (c) The accumulated phase of the center electron spin (and thus the measurement strength of the weakly coupled target nuclear spin) is controlled by the pulse number of the applied CPMG sequence.

$$H = \frac{\sigma_z}{2} \otimes \beta + H_0, \tag{2}$$

where $\sigma_z = |1\rangle\langle 1| - |0\rangle\langle 0|$ is the Pauli operator (hereafter $|1\rangle$ denotes $|-1\rangle$), $\beta = \mathbf{A}\cdot\hat{\mathbf{I}}$ is the noise operator, and $H_0 = (\mathbf{A}/2)\cdot\hat{\mathbf{I}} + \gamma_n \mathbf{B}\cdot\hat{\mathbf{I}} = \omega \mathbf{n}_{\parallel}\cdot\hat{\mathbf{I}}$ is the effective Hamiltonian for the ^{13}C nuclear spin. With the unit vector $\mathbf{n}_{\parallel}$ on the direction of H_0, $\mathbf{A}$ can be decomposed as $A_{\perp} = |\mathbf{A} - (\mathbf{A}\cdot\mathbf{n}_{\parallel})\mathbf{n}_{\parallel}|$. For a weakly coupled nuclear spin ($A_{\perp} \ll \omega$), consider the Carr-Purcell-Meiboom-Gill (CPMG) control with π flips at time $t_p = (2p-1)\tau$ (where 2τ is the interval between pulses and $p = 1, 2, \ldots, N$), using the Magnus expansion [29,30], we obtain the nuclear spin propagator conditioned on the NV electron spin state as [31]

$$U^N_{(\pm)}(t) = \exp(-i\omega I_{\parallel} t)\exp\left[\mp \frac{iA_{\perp}}{2\omega} F(\omega, t) I_{\perp}\right], \tag{3}$$

where $F(\omega,t) = |\sum_{p=0}^{N}(-1)^p(e^{-i\omega t_{p+1}} - e^{-i\omega t_p})|$ is the DD filter function, $I_{\parallel/\perp} = \mathbf{n}_{\parallel/\perp}\cdot\hat{\mathbf{I}}$ with $\mathbf{n}_{\perp} = [\mathbf{A} - (\mathbf{A}\cdot\mathbf{n}_{\parallel})\mathbf{n}_{\parallel}]/A_{\perp}$. The subscript +(-) denotes the propagator starting from the $|0\rangle$ ($|1\rangle$) state of the electron spin.

In general, the DD sequence steers the quantum evolution of a target nuclear spin, and the initial state and final states of the target nuclear spin under DD sequence are not the same [8,28]. Nonetheless, we find that at the resonance points of ω, i.e., $\tau = \pi/(2\omega)$, the eigenstates of $I_{\perp}$ remain in the same state after the CPMG control with an even pulse number N [31]. We denote them as $\{|\uparrow\rangle, |\downarrow\rangle\}$, which satisfy

$$U^N_{(\pm)}(N\pi/\omega)|\uparrow\rangle = (-1)^{(N/2)} e^{\mp iN\phi}|\uparrow\rangle, \tag{4}$$

$$U^N_{(\pm)}(N\pi/\omega)|\downarrow\rangle = (-1)^{(N/2)} e^{\pm iN\phi}|\downarrow\rangle, \tag{5}$$

where $\phi = A_{\perp}/(2\omega)$ is the accumulated phase by the nuclear spin during the pulse delay 2τ. Since those nuclear spin states remain the same before and after CPMG sequence, we can repetitively map and read out their quantum states with the help of the ancillary electron spin, and realize the single-shot readout of the target nuclear spin.

Besides the effect of locking the nuclear spin to the $\{|\uparrow\rangle, |\downarrow\rangle\}$ states, the CPMG sequence can tune the measurement strength of the target nuclear spin. The center electron spin, which is first prepared to the superposition state of $\Psi_0 = (1/\sqrt{2})(|0\rangle + |1\rangle)$, accumulates a phase determined by the state of the target nuclear spin and the pulse number of CPMG sequence, as illustrated in Fig. 1(c). After N pulse CPMG sequence, the final state of electron spin is $\Psi_{\uparrow} = (1/\sqrt{2})(|0\rangle + e^{i2N\phi}|1\rangle)$ for the nuclear spin $|\uparrow\rangle$ state or $\Psi_{\downarrow} = (1/\sqrt{2})(|0\rangle + e^{-i2N\phi}|1\rangle)$ for the nuclear spin $|\downarrow\rangle$ state. In particular, if the pulse number N is such that $2N\phi = \pi/2$, the final state of the two-qubit system is $|0\downarrow\rangle$ or $|1\uparrow\rangle$ after the application of a Hadamard gate to the electron spin. Thus, a maximum entanglement between the center electron spin and the target nuclear spin can be established. As a comparison, when the pulse number is small, the nuclear spin is only weakly entangled with the ancillary electron spin, so a projective measurement of the electron spin will only cause partial collapse of the nuclear spin and hence a weak measurement on the nuclear spin [10,36].

We experimentally demonstrate our protocol on an NV center in a high-purity type-IIa diamond. As seen in the ODMR spectrum of the NV center [31], there is no apparent splitting due to hyperfine interaction with strongly coupled ^{13}C nuclear spin. As a confirmation of the absence of strongly coupled ^{13}C spins, the coherence in the Hahn echo (CPMG-1) presents no oscillation features. Under multipulse DD control (CPMG-12), however, the measured coherence presents an extended plateau and a number of dips, as shown in Fig. 1(b). So this NV center does have a few ^{13}C nuclear spins located nearby but with weak hyperfine interaction. By fitting the CPMG signal from different initial states of the center electron spin $(1/\sqrt{2})(|0\rangle + |\pm 1\rangle)$, we derived that the hyperfine interaction of the nearest ^{13}C nuclear spin projected along the quantization axis of NV electron spin is about 330 kHz. Other nuclear spins have coupling strength less than this [31]. For all those nuclear spins ($|A| < (1/T_2^*) \approx 2$ MHz), if taken as qubits, cannot be read out in a single shot in traditional protocols.

The gradually enhanced entanglement between the NV center spin and a certain ^{13}C nuclear spin is evidenced by the increasing depth of the coherence dip under more and more control pulses. As shown in Fig. 2, under an external magnetic field of 305 G, when the pulse interval matches the half precession period of an individual nuclear spin (e.g., $\tau = 456$ ns), the accumulated phase in each interval has the same direction, and the coherence dip has increasing depth with increasing the number of intervals. Actually, when the number of pulses N is further increased, the overshoot evolution of the nuclear spin can cause the disentanglement and, hence, the recovery of the central spin coherence. This coherence recovery effect unambiguously demonstrates the quantum nature of the noise source, i.e., the ^{13}C nuclear spin [37]. Maximum entanglement between the electron and nuclear spins is reached when the pulse interval τ and the number of pulses N are such that the central spin coherence exactly vanishes. For a certain target nuclear spin (a fixed τ), if it is in the fully mixed state with density matrix $\rho = 1/2$ (not polarized), the NV electron spin coherence shows oscillation behavior when the CPMG pulse number is increased [29], i.e.,

$$\mathcal{L}_{\mathrm{dip}}(N) \approx \cos\left(\frac{A_\perp N}{\omega}\right). \tag{6}$$

The oscillation feature of the center spin coherence presented in Fig. 2(c) is due to entanglement and disentanglement with the closest ^{13}C nuclear spin, which has $A_\perp = 200$ and $\omega = 517$ kHz under the magnetic field (305 G). The measured period of coherence oscillate is $N = 16$, which agrees well with the theory prediction of $N = 2\pi\omega/A_\perp = 16.3$ [31].

Since the nuclear spin state is locked during the periodic driving of CPMG, we can repeat many cycles of measurement on the electron spin to accumulate sufficient statistical confidence and, thus, achieve single-shot readout of the target nuclear spin. As shown in Fig. 3, under an external magnetic field of 691 G, we use a CPMG-12 sequence with resonant τ of 252 ns and a following optical pulse (300 ns) to read out the closest nuclear spin [corresponds to the first coherence dip in Fig. 1(b)]. A short waiting interval is added after the readout and reinitialization of electron spin to make the measurement duration match the precession period of target nuclear spin (≈ 1 μs under this magnetic field). The photon counts in 40 000 cycles (in 189 ms) are summed together to a single data point, which presents the state of the nuclear spin under measurement.

With the single-shot measurement, we are able to directly observe the quantum jumps of the target nuclear spin. Typical photon count trace is shown in Fig. 3(b). Two distinct values are clearly seen. We associate the high (low) count rate to the $|\uparrow\rangle$ ($|\downarrow\rangle$) state of the target nuclear spin. A relaxation time (T_{1n}) of about 15 second for both $|\uparrow\rangle$ and $|\downarrow\rangle$ states is measured ($B = 691$ G). The initialization and

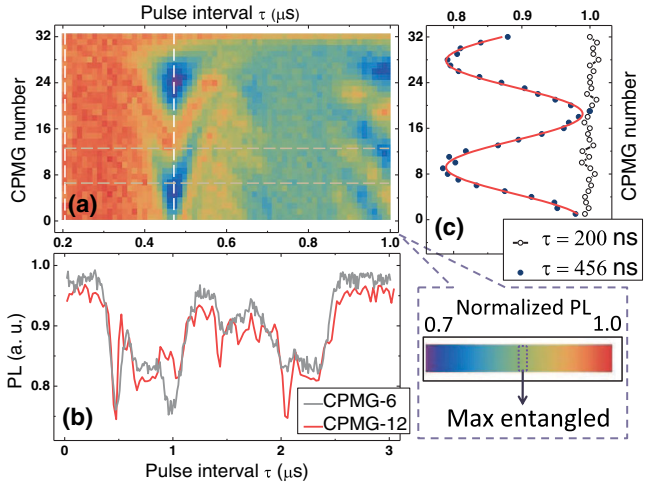

FIG. 2. Controlling the strength of measurement on a weakly coupled nuclear spin by dynamical decoupling. (a) 2D CPMG signal as a function of the pulse number and the interval duration, under an external magnetic field of 305 G. Individual nuclear spins are selected by tuning the intervals between two CPMG pulses. The number of total applied pulses determines the measurement strength of the selected nuclear spin. (b) Typical CPMG signal as a function of the interval duration. (c) Typical CPMG signal as a function of the pulse number. When no nuclear spin is resonant ($\tau = 200$ ns, black line), the coherence of the center spin is well protected. When a nuclear spin is resonantly selected ($\tau = 456$ ns, red line with blue point), the coherence of the electron spin is modulated by the entanglement with the nuclear spin.

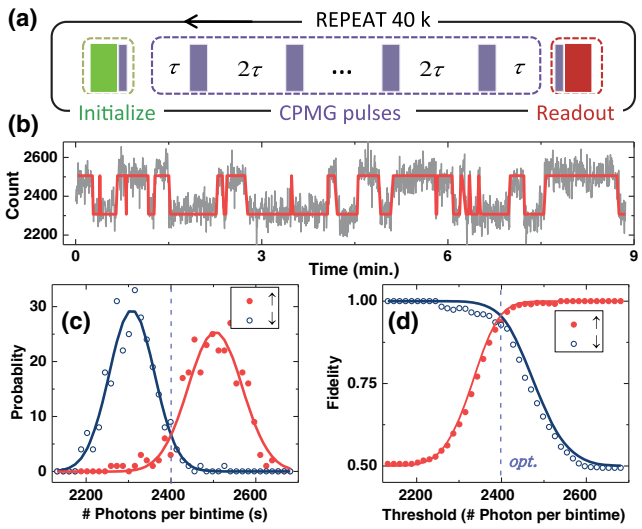

FIG. 3. Single-shot readout of a weakly coupled nuclear spin. (a) Pulse sequence. The weakly coupled nuclear spin is selectively addressed by CPMG pulses with resonant τ, and a subsequent optical readout reveals the state of the target nuclear spin. (b) Typical quantum jump signal of the weakly coupled nuclear spin under an external magnetic field of 691 G. Each data point is a sum of 40 000 cycles of measurement of the center electron spin. (c) Photon count distributions after the target nuclear spin state selected by the photon count thresholds of < 2300 for $|\downarrow\rangle$ and > 2520 for $|\uparrow\rangle$. (d) Single-shot readout fidelity as a function of the readout threshold. With a threshold of 2400, the readout fidelity is 95.5% for both $|\downarrow\rangle$ and $|\uparrow\rangle$.

readout fidelity of our single-shot readout protocol is estimated as following Ref. [21] and presented in Figs. 3(c)–3(d). The photon count distributions for the nuclear spin state being initialized to the $|\uparrow\rangle$ and $|\downarrow\rangle$ states are well distinguished. For a threshold of 2400, which is the maximum overlap between the photon counting distributions for the two nuclear spin states, the readout fidelity is 95.5% (for both $|\uparrow\rangle$ and $|\downarrow\rangle$ states, see Supplemental Material [31] for details). The fidelity can be further improved by increasing the photon collection efficiency and the fidelity of the electron spin manipulation.

The dynamic of the target nuclear spin under repetitive measurements is revealed by numerical simulation. The density matrix of the nuclear spin after the nth repetition of CPMG sequence is depicted as $\rho_n = \frac{1}{2}(1 + r_n \mathbf{e} \cdot \hat{\boldsymbol{\sigma}})$, where $r_n\mathbf{e}$ is the Bloch vector and represents its polarization. Several trajectories, simulated with realistic hyperfine tensor and the experimental parameters of P_1 ($B = 691$ G, $N = 12$, and $\tau = 252$ ns) and P_2 ($B = 305$ G, $N = 12$, and $\tau = 456$ ns), are presented in Fig. 4(a). Starting from a mixed state $\rho_0 = 1/2$, the nuclear spin is steered by the backaction of repetitive measurements and settles down as one of the CPMG-locked states $\{|\uparrow\rangle, |\downarrow\rangle\}$ is achieved. Under relatively strong measurement of P_2, this is achieved in 3 steps. As a comparison, weak measurements of the P_1 condition take several tens of steps. Nevertheless, the collapse process is very short compared with the total repeat number (40 000). It is worth noting that the probability of choosing which trajectory to collapse is determined by the initial state of the nuclear spin and the state collapse process is effectively a projective measurement of the target nuclear spin.

After the primal collapse process, the nuclear spin state is trapped in the following measurements, which make this scheme robust to experimental imperfections. The CPMG locked states $\{|\uparrow\rangle, |\downarrow\rangle\}$ behave as attractors in the nuclear spin Bloch sphere, sparse deviations from them would be corrected in subsequent measurements. Meanwhile,

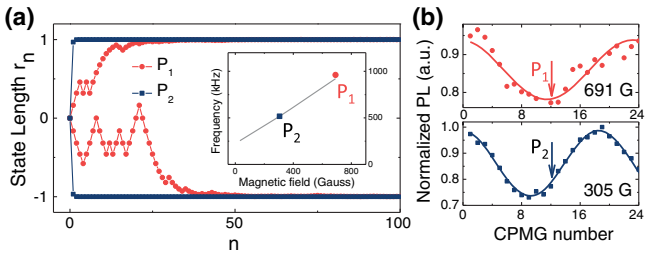

FIG. 4. Trajectory of nuclear spin state under repetitive weak measurements. (a) Samples of trajectory, calculated with realistic hyperfine tensor. Red circles are for relative weak measurements (P_1), about 40 steps are needed to reach the stable state $\{|\uparrow\rangle, |\downarrow\rangle\}$; Navy square are for relative strong measurement (P_2). Inset, dependence of the target nuclear spin precession frequency on magnetic field strength (solid line). P_1 and P_2 are experimental optimized conditions to observe jump signal. (b) The positions of P_1 and P_2 in CPMG parameter space.

numerical simulation reveals that mismatching of the resonant condition (due to discrete time resolution in experiments) can be compensated by the readout duration [38]. The nuclear spin state is stable under millions of CPMG repetitions with realistic experimental parameters [31]. Quantum jumps are observed for both the P_1 and P_2 conditions in experiments (data in Fig. 3 and Fig. S6 of Ref. [31], respectively). The optimized pulse interval τ exactly matches the precession frequency of the target nuclear spin, as shown in the inset of Fig. 4(a), which confirms that the jump signal indeed comes from the weakly coupled ^{13}C nuclear spin.

The observed quantum jumps at room temperature indicate that the weakly coupled nuclear spin is a robust quantum bit even under the nonresonant optical excitation, which is consistent with former experiments [4]. The NV excited states $|A_1\rangle$, $|A_2\rangle$, $|E_1\rangle$, $|E_2\rangle$ contain the component of both $|-1\rangle, |+1\rangle$ while $|E_x\rangle, |E_y\rangle$ includes only spin $|0\rangle$ component [39]. Under optical excitation, the indirect coupling of the electron spin $|-1\rangle, |+1\rangle$ states brings random phase to the target nuclear spin. Fortunately, the optical transition rates are much larger than the dipole interaction between electron spin and the target nuclear spin, so the magnetic noise from electron spin would be dramatically suppressed due to the effect analogous to motional averaging [40,41].

The DD-enabled single-shot readout of a weakly coupled nuclear spin largely extends the range of physical systems for scalable quantum computing. We note that the stationary nuclear spin states can be continuously tuned in the equatorial circumstance of the Bloch sphere if phase-shifted CPMG pulse sequence is employed, and the z axis of the Bloch sphere can be tuned by the external magnetic field, so, in principle, an arbitrary state in the Bloch sphere can be readout by the NV electron spin under phase-shifted CPMG control [8,31].

In conclusion, we propose and demonstrate a scheme of single-shot readout of a weakly coupled nuclear spin at room temperature. The projective measurement of the target nuclear spin is implemented by repetitively applying dynamical decoupling and subsequent nonresonant optical readout on an ancillary electron spin. This scheme is easy to be implemented in experiment and robust to pulse errors. For the selected target nuclear spin, the measurement strength is tunable by adjusting the CPMG number; thus, both strong and weak measurement can be achieved for the same system. Weak measurement of a quantum system is of particular interest since the target system can be steered through the backaction of sequential weak measurements and real-time feedback [10,42,43]; together with the demonstrated single-shot readout scheme, it is possible to demonstrate measurement-only quantum computing in an NV system at room temperature.

The authors acknowledge F. Jelezko, P. Huang, X. Kong, and F. H. Zhang for helpful discussions. This work was supported by the National Basic Research Program of China under Grants No. 2014CB921402 and

No. 2015CB921103, the Strategic Priority Research Program of the Chinese Academy of Sciences under Grant No. XDB07010300, the National Natural Science Foundation of China under Grant No. 11574386, Hong Kong Research Grants Council—Collaborative Research Fund Project CUHK4/CRF/12G, and The Chinese University of Hong Kong Vice Chancellor's One-off Discretionary Fund.

*xypan@aphy.iphy.ac.cn

[1] B. E. Kane, Nature (London) **393**, 133 (1998).
[2] P. Neumann, J. Beck, M. Steiner, F. Rempp, H. Fedder, P. R. Hemmer, J. Wrachtrup, and F. Jelezko, Science **329**, 542 (2010).
[3] F. Jelezko, T. Gaebel, I. Popa, M. Domhan, A. Gruber, and J. Wrachtrup, Phys. Rev. Lett. **93**, 130501 (2004).
[4] P. C. Maurer, G. Kucsko, C. Latta, L. Jiang, N. Y. Yao, S. D. Bennett, F. Pastawski, D. Hunger, N. Chisholm, M. Markham *et al.*, Science **336**, 1283 (2012).
[5] J. J. Morton, A. M. Tyryshkin, R. M. Brown, S. Shankar, B. W. Lovett, A. Ardavan, T. Schenkel, E. E. Haller, J. W. Ager, and S. Lyon, Nature (London) **455**, 1085 (2008).
[6] J. J. Pla, K. Y. Tan, J. P. Dehollain, W. H. Lim, J. J. Morton, F. A. Zwanenburg, D. N. Jamieson, A. S. Dzurak, and A. Morello, Nature (London) **496**, 334 (2013).
[7] G. Waldherr, Y. Wang, S. Zaiser, M. Jamali, T. Schulte-Herbrüggen, H. Abe, T. Ohshima, J. Isoya, J. Du, P. Neumann *et al.*, Nature (London) **506**, 204C (2014).
[8] T. H. Taminiau, J. Cramer, T. van der Sar, V. V. Dobrovitski, and R. Hanson, Nat. Nanotechnol. **9**, 171 (2014).
[9] P. Neumann, N. Mizuochi, F. Rempp, P. Hemmer, H. Watanabe, S. Yamasaki, V. Jacques, T. Gaebel, F. Jelezko, and J. Wrachtrup, Science **320**, 1326 (2008).
[10] M. Blok, C. Bonato, M. Markham, D. Twitchen, V. Dobrovitski, and R. Hanson, Nat. Phys. **10**, 189 (2014).
[11] L. Jiang, J. Hodges, J. Maze, P. Maurer, J. Taylor, D. Cory, P. Hemmer, R. Walsworth, A. Yacoby, A. Zibrov *et al.*, Science **326**, 267 (2009).
[12] D. P. DiVincenzo, Fortschr. Phys. **48**, 771 (2000).
[13] R.-B. Liu, W. Yao, and L. Sham, Adv. Phys. **59**, 703 (2010).
[14] L. Robledo, L. Childress, H. Bernien, B. Hensen, P. F. Alkemade, and R. Hanson, Nature (London) **477**, 574 (2011).
[15] W. Pfaff, T. H. Taminiau, L. Robledo, H. Bernien, M. Markham, D. J. Twitchen, and R. Hanson, Nat. Phys. **9**, 29 (2013).
[16] J. Cramer, N. Kalb, M. A. Rol, B. Hensen, M. S. Blok, M. Markham, D. J. Twitchen, R. Hanson, and T. H. Taminiau, Nat. Commun. **7**, 11526, (2016).
[17] N. Kalb, J. Cramer, D. Twitchen, M. Markham, R. Hanson, and T. Taminiau, Nat. Commun. **7**, 13111, (2016).
[18] A. Reiserer, N. Kalb, M. S. Blok, K. J. M. van Bemmelen, T. H. Taminiau, R. Hanson, D. J. Twitchen, and M. Markham, Phys. Rev. X **6**, 021040 (2016).
[19] S. Yang, Y. Wang, D. B. Rao, T. H. Tran, A. S. Momenzadeh, M. Markham, D. Twitchen, P. Wang, W. Yang, R. Stöhr *et al.*, Nat. Photonics **10**, 507 (2016).
[20] G. Waldherr, J. Beck, M. Steiner, P. Neumann, A. Gali, T. Frauenheim, F. Jelezko, and J. Wrachtrup, Phys. Rev. Lett. **106**, 157601 (2011).
[21] A. Dréau, P. Spinicelli, J. R. Maze, J.-F. Roch, and V. Jacques, Phys. Rev. Lett. **110**, 060502 (2013).
[22] N. Zhao, J.-L. Hu, S.-W. Ho, J. T. Wan, and R. Liu, Nat. Nanotechnol. **6**, 242 (2011).
[23] N. Zhao, J. Honert, B. Schmid, M. Klas, J. Isoya, M. Markham, D. Twitchen, F. Jelezko, R.-B. Liu, H. Fedder *et al.*, Nat. Nanotechnol. **7**, 657 (2012).
[24] S. Kolkowitz, Q. P. Unterreithmeier, S. D. Bennett, and M. D. Lukin, Phys. Rev. Lett. **109**, 137601 (2012).
[25] T. H. Taminiau, J. J. T. Wagenaar, T. van der Sar, F. Jelezko, V. V. Dobrovitski, and R. Hanson, Phys. Rev. Lett. **109**, 137602 (2012).
[26] F. Shi, X. Kong, P. Wang, F. Kong, N. Zhao, R.-B. Liu, and J. Du, Nat. Phys. **10**, 21 (2014).
[27] N. Zhao, S.-W. Ho, and R.-B. Liu, Phys. Rev. B **85**, 115303 (2012).
[28] G.-Q. Liu, H. C. Po, J. Du, R.-B. Liu, and X.-Y. Pan, Nat. Commun. **4**, 2254 (2013).
[29] W.-L. Ma and R.-B. Liu, Phys. Rev. Applied **6**, 024019 (2016).
[30] A. Albrecht and M. B. Plenio, Phys. Rev. A **92**, 022340 (2015).
[31] See Supplemental Material at http://link.aps.org/supplemental/10.1103/PhysRevLett.118.150504 for the detailed theoretical description and numerical simulation of our scheme, as well as the experimental results of quantum jumps at $B = 305$ G, which includes Refs. [32–35].
[32] J. R. Maze, J. M. Taylor, and M. D. Lukin, Phys. Rev. B **78**, 094303 (2008).
[33] G.-Q. Liu, X.-Y. Pan, Z.-F. Jiang, N. Zhao, and R.-B. Liu, Sci. Rep. **2**, 432 (2012).
[34] L. Childress, M. G. Dutt, J. Taylor, A. Zibrov, F. Jelezko, J. Wrachtrup, P. Hemmer, and M. Lukin, Science **314**, 281 (2006).
[35] W. Yang, Z.-Y. Wang, and R.-B. Liu, Frontiers Phys. China **6**, 2 (2011).
[36] Y. Aharonov, D. Z. Albert, and L. Vaidman, Phys. Rev. Lett. **60**, 1351 (1988).
[37] N. Zhao, J. Honert, B. Schmid, M. Klas, J. Isoya, M. Markham, D. Twitchen, F. Jelezko, R.-B. Liu, H. Fedder *et al.*, Nat. Nanotechnol. **7**, 657 (2012).
[38] W. Ping (unpublished).
[39] M. W. Doherty, N. B. Manson, P. Delaney, and L. C. Hollenberg, New J. Phys. **13**, 025019 (2011).
[40] L. Jiang, M. V. G. Dutt, E. Togan, L. Childress, P. Cappellaro, J. M. Taylor, and M. D. Lukin, Phys. Rev. Lett. **100**, 073001 (2008).
[41] P. Wang and W. Yang, New J. Phys. **17**, 113041 (2015).
[42] K. Murch, S. Weber, C. Macklin, and I. Siddiqi, Nature (London) **502**, 211 (2013).
[43] S. Weber, A. Chantasri, J. Dressel, A. Jordan, K. Murch, and I. Siddiqi, Nature (London) **511**, 570 (2014).